Proceedings of the 9th International Conference on Fluid Flow, Heat and Mass Transfer (FFHMT'22)
Niagara Falls, Canada – June 08-10, 2022
Paper No. 211
DOI: 10.11159/ffhmt22.211

CFD Modelling Of Film Deposition from a Receding Meniscus in a Capillary Tube Using the Approach of Overset Grid Technique

Alihossein Nikkhah[1], Nooshin Karami[1], Albert Tessier-Poirier[1], Omid Abouali[2], Luc G. Fréchette[1]
[1]Institut Interdisciplinaire d'Innovation Technologique (3IT), Univ. de Sherbrooke
Sherbrooke, QC, Canada
Alihossein.Nikkhah@usherbrooke.ca; Nooshin.Karami@usherbrooke.ca; Albert.tessier-poirier@usherbrooke.ca
Luc.Frechette@usherbrooke.ca
[2]School of Mechanical Engineering, Shiraz University, Shiraz, Iran
abouali@shirazu.ac.ir

Abstract **–** Meniscus motion in a capillary tube is a very common type of flow in thermal management devices such oscillating and pulsating heat pipes. It is well known, that the thin film deposited on the wall, which is due to liquid shear force, plays a major role in heat and mass transfer of those devices. This study focuses on the hydrodynamics of this flow using a CFD axisymmetric model of a 1mm diameter capillary, with the approach of volume of fluid (VoF). The CFD-VOF approach is tuned to capture the liquid film deposition from a receding meniscus at different constant velocities. Due to high required grid resolution, the moving overset mesh technique is used. In doing so, a fine meshed domain consists of meniscus slides over the background domain with a coarse mesh. By using this technique, the number of cells and computational time reduced considerably in comparison with regular meshing approach. With water as a working fluid, the numerical results for the liquid film thickness, at different velocities, compare well with experimental data from the literature. The simulations also show that at higher capillary number, the axial location where the film thickness becomes constant moves away from the meniscus nose. The shear stress distribution indicates higher values near the meniscus compared to uniform film and liquid plug zones which is due to the interface curvature in this zone. Also, a recirculating flow was observed within the liquid film left behind the receding meniscus which could have favourable effects in terms of heat and mass transfer. The present work on hydrodynamics is the first step toward complete modelling of an oscillating meniscus with mass and heat transfer inside the capillaries.

Keywords**:** Computational fluid dynamic (CFD), overset grid, self-oscillating fluidic heat engine (SOFHE), Oscillating heat pipe (OHP), wetting dynamic

Nomenclature

		α_l	Liquid volume fraction
$\overrightarrow{F_\sigma}$	Surface tension source term (N/m^3)	α_a	Air volume fraction
$\vec{V}$	Flow velocity vector (m/s)	κ	interface curvature (1/m)
Ub	Boundary velocity (m/s)	μ	Dynamic viscosity (kg/m/s)
Um	Meniscus velocity (m/s)	ϑ	Kinematic viscosity (m^2/s)
P_0	Amplitude of pressure oscillation (Pa)	ρ	Density (kg/m^3)
Ca	Capillary number	σ	Surface tension coefficient (N/m)

1. Introduction

Thermal management devices such as oscillating and pulsating heat pipes (OHP and PHP)[1], [2] as well as recent thermofluidic energy harvesters such as SOFHE[3], are two phase flow devices which includes moving menisci and employs phase transition (evaporation and condensation) for operation. Generally, there are two main physical phenomena in the study of SOFHE and OHP/PHP, which are the hydrodynamic aspects as well as exchange of heat and mass transfer between phases. Understanding these aspects, is the keystone in improving the performance of these devices.

Regarding the hydrodynamic aspects, a liquid film is left on the wall as a meniscus recedes in a capillary tube, due to viscous shear forces. This liquid film plays a major role in the operation of those devices as it provides the available liquid

with low thermal resistance for evaporation [4]–[7]. With the assumption of a flat surface over the liquid film on the wall, the lubrication approximation of the hydrodynamics equation yields acceptable results in terms of film thickness[8]. However, this assumption fails to be valid for the meniscus and the de-wetting ridge due to curvature of the film, and its validity is also questionable for the evaporating liquid film. As a result, higher order numerical approaches like CFD are required to capture the more complex flow features. However, CFD modelling of meniscus motion and film deposition can be very time consuming as it requires high grid resolution specially in the case of large distance movement or amplitude of the meniscus. To the best of our knowledge, no specific CFD modelling of meniscus wetting dynamics inside a capillary has been presented in the literature.

The purpose of the current research is to define a CFD model which is capable of capturing the wetting dynamics of a receding meniscus, focusing on the liquid film thickness left on the wall. In doing so, the CFD technique with the approach of volume of fluid (VoF) has been used, in combination with a moving mesh. The numerical results of the liquid film thickness left behind receding meniscus at different constant velocities has been validated with experimental data reported in literature [9] to tune the hydrodynamic CFD model. Instead of using high grid resolution along the length of the capillary, the moving overset grid approach is used to follow the meniscus region in order to reduce the number of cells and the computational time. In fact, this is the first step toward accurate CFD modelling of an oscillating meniscus with phase transition.

2. Physical Model

2.1. Governing equations and constitutive relations

The volume of fluid (VOF) is a multiphase modelling approach used for modelling of dominantly immiscible fluids which have clear interfaces between them. In the current modelling, there are two phases, water and air, in contact in a capillary tube, and their interface (meniscus) is assumed to be continuous and immiscible. In this regard the VOF technique is used to track the meniscus. In doing so, the parameter of volume fraction, α_i, is introduced and assigned to each phase, which is the volume fraction of a cell occupied by phase i (liquid water or air). According to their definitions, the volume fractions in each computational cell sum to unity Eq. (1). The cells on the interface are occupied by both liquid water and air phases while on the two sides of interface, ideally, it's supposed to have only one phase. As in single-phase laminar flow, here a single momentum set of equations Eq. (2) and a continuity equation Eq. (3) are solved for the entire domain. However, the way the fluid properties are calculated as well as the interface force source term $\overrightarrow{F_\sigma}$ in the momentum equation Eq. (2) distinguishes it from a single-phase flow.

$$\alpha_l + \alpha_a = 1 \tag{1}$$

$$\frac{\partial \rho \vec{V}}{\partial t} + \nabla.\left(\rho \vec{V}\vec{V}\right) = -\nabla P + \nabla.\left[\mu(\nabla \vec{V} + \nabla \vec{V}^T)\right] + \overrightarrow{F_\sigma} \tag{2}$$

$$\frac{\partial \rho}{\partial t} + \nabla.\left(\rho \vec{V}\right) = 0 \tag{3}$$

For the fluid properties in Eqs. (2)-(3), the volume average of the existing fluid phase's properties is used in each computational cell as in Eq. 4. For this purpose, the phase's volume fractions are required, which necessitates adding another continuity equation for one of the phases (Eq. (5), so- called interface tracking equation). This phase is referred to as a secondary phase, and chosen as the liquid water in the current research.

$$\rho = \alpha_l \rho_l + \alpha_a \rho_a$$
$$\mu = \alpha_l \mu_l + \alpha_a \mu_a \tag{4}$$

$$\frac{\partial(\alpha_l \rho_l)}{\partial t} + \nabla.\left(\alpha_l \rho_l \vec{V}\right) = 0 \tag{5}$$

Moreover, air phase is considered as an ideal compressible gas, which obeys the perfect gas law. The source term $\overrightarrow{F_\sigma}$ in the momentum balance equation is considered to capture the effect of the surface tension which was proposed by Brackbill [10] and acts when both phases are present at a computational cell. Surface tension is applied at the interface, and is converted to a volume force Eq. (6) by applying the divergence theorem to use it in the momentum equation as a source.

$$\overrightarrow{F_\sigma} = \sigma_{al} \frac{\kappa_l \rho_l \overrightarrow{\nabla \alpha_l}}{0.5(\rho_l + \rho_v)} \tag{6.1}$$

$$\kappa_l = \nabla.\left(\frac{\overrightarrow{\nabla \alpha_l}}{\left|\overrightarrow{\nabla \alpha_l}\right|}\right) \tag{6.2}$$

2.2. Domain discretization and boundary conditions

As the governing equations cannot be solved analytically, they will be discretized in time and space to form a set of equations which are solved by the appropriate approaches in computation fluid dynamics. To do so, the computational domain consists of a 0.5mm×100mm rectangle representing an axisymmetric section of a circular tube, discretized into small cells. As a result, there is no real sharp interface between the two immiscible fluids but the interface has a finite thickness depending on the grid resolution. Although with higher grid resolution, the results are more accurate, the computational time is also higher which is not desired. To address this problem, the over set technique is used. As indicated in Fig. 1, the moving meshed box which has the priority for computations to be done on, slides over a background mesh and follows the meniscus to enhance the accuracy near the high gradient of volume fraction regions. In this regard, the gradient of volume fraction far enough from the meniscus is normal to the wall [8] so that there is no need to have high resolution mesh parallel to the wall. The data transfer between the component and the background meshes is performed through the overset interfaces where both fine and coarse meshes of the component and background meshes exist at the same time. A boundary layer meshed zone is considered normal to the wall in both component and background meshes which coincide with the direction normal to the wall to avoid the interpolation of the flow data in that direction.

2.3. Numerical procedure and boundary conditions

Ansys Fluent 19R3 solver with the volume of fluid method have been used to model the liquid film deposition on the wall. In this regard, the pressure-velocity coupling is obtained by the implicit method of coupled in the solver as it is currently the only compatible approaches with overset grid. The PRESTO scheme is used for the pressure interpolation and the schemes of second order upwind and Geo-Reconstruct are used for discretizing the momentum and volume fraction equations, respectively. To follow the meniscus, the sliding component grid moves over the background mesh according to the location of the maximum absolute value of the volume fraction gradient on the axis of the tube. A user defined function (UDF) has been developed to control the motion of the sliding component. A variable time-stepping method is used for the transient simulation based on the value of 0.5 for the global Courant number. As a result, the time step size is smaller for higher meniscus velocity, which is desired.

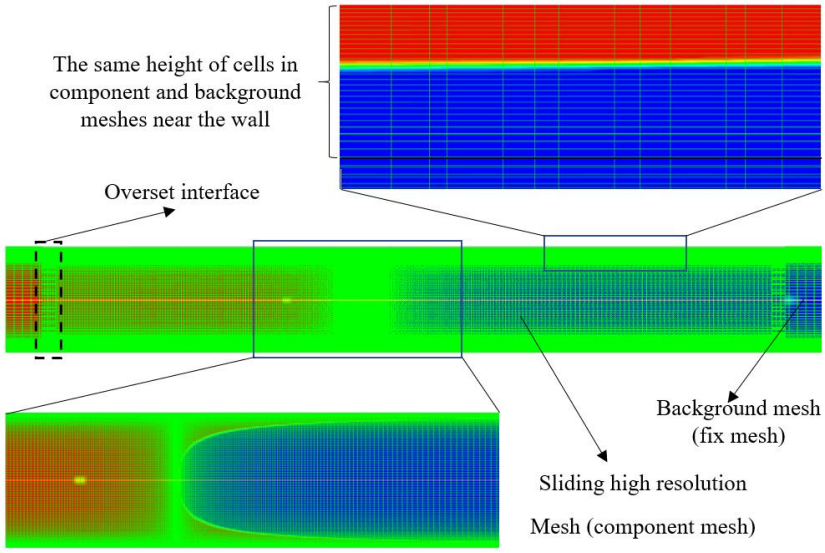

Fig. 1: Overset grid generation and components

3. Results and Discussion

3.1. Validation of numerical results

The accuracy of the numerical results is validated by comparison with experimental data for the liquid film thickness, reported at steady condition by Youn et al. [9]. To compare the numerical results with the experimental data, in addition to material properties and the tube geometry, the meniscus velocity should be the same for both cases. However, the meniscus velocity, which is the main dynamic property affecting the film thickness, is a part of the solution not an input in the CFD analysis and is determined iteratively by trying different values for boundary velocity, Ub (the velocity at pipe inlet which is an input in CFD and equal to mean volumetric velocity). As shown in Fig. 2, the obtained numerical velocities, Um_numerical, for the meniscus are very close to the measured experimental data, Um_experimental. So, the numerical and experimental results for the film thickness are comparable. Fig. 2 also shows the diagram of the boundary velocity Ub, versus the meniscus velocity, U_m. Due to the deposited liquid film on the wall, U_m is always higher than U_b to make the mass of liquid conserved.

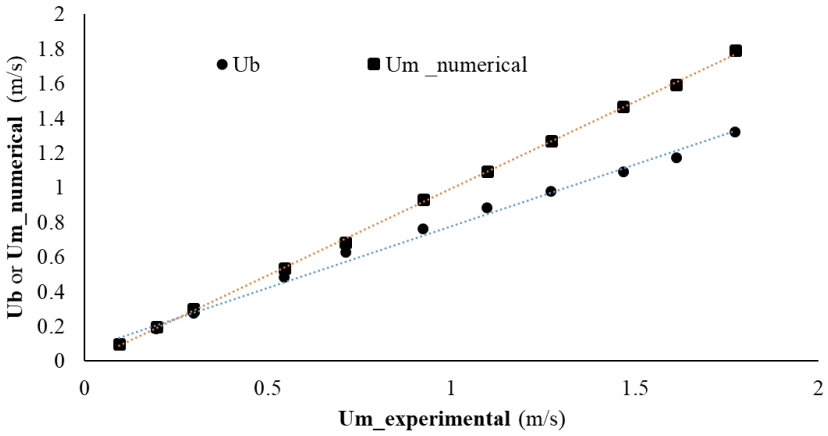

Fig. 2: Numerical boundary and meniscus velocities (Ub and Um_numerical) versus experimental meniscus velocity (Um_experimental)

To numerically measure the film thickness, as shown in Fig. 3, the maximum radial gradient of the volume fraction is used to locate the position of the interface since we expect the real location of the interface to happen at the maximum change of the volume fraction. The values of the volume fraction that correspond to the location of maximum gradient for all sections along the pipe are close to 0.5, which is coherent.

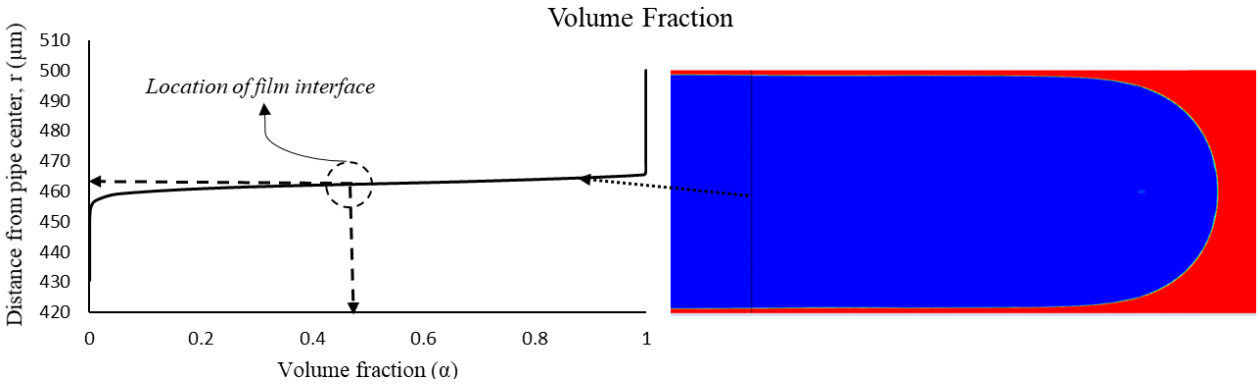

Fig. 3: Numerical measurement of the film thickness

In Fig. 4, the extracted film thickness at different sections behind the receding meniscus is plotted for two different capillary numbers. As presented in Fig. 4, the asymptotic value is chosen as for the film thickness at Ca=0.0075 and Ca=0.015. The film profile at higher capillary numbers moves away from the meniscus nose. In other words, the meniscus approaches the film region more gradually at higher capillary numbers. In addition, the axial location of the initial film thickness is four diameters away from the meniscus nose at Ca=0.015 while it reduces to almost one diameter away at Ca=0.0027. This indicates that the shear force has a longer effective range at higher capillary numbers.

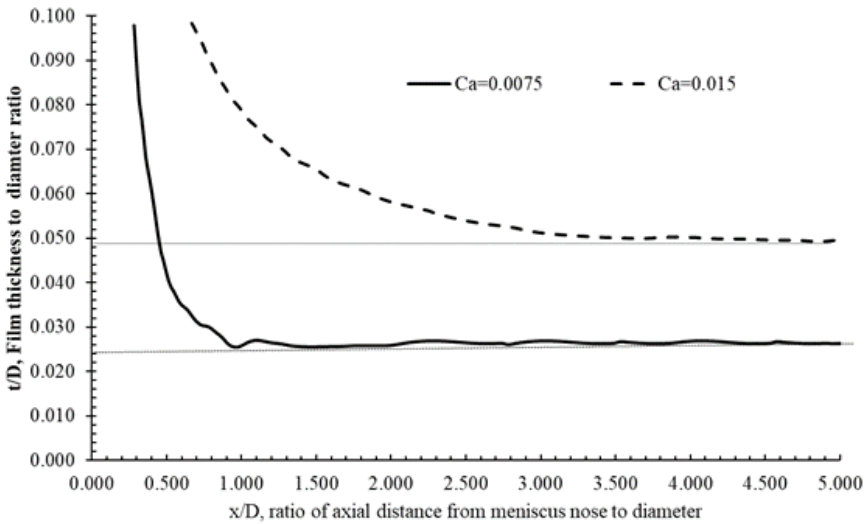

Fig 4: Liquid film profile for Ca=0.0075 and Ca=0.015

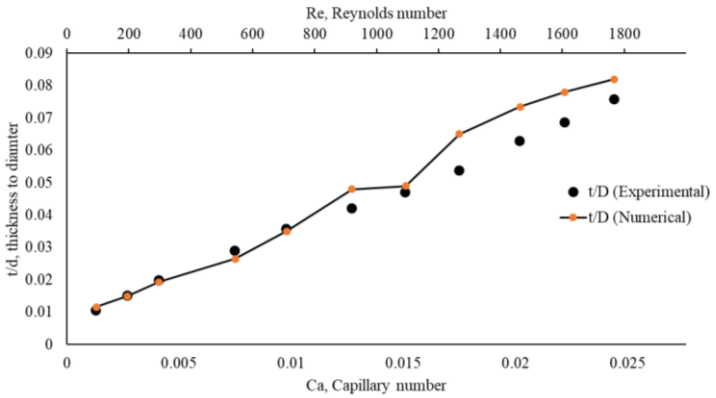

Fig. 5: Validation of the predicted thickness of the deposited liquid film by CFD with experimental measurements

3.2. Flow Pattern and Shear Stress

The deposited liquid film is the result of force balance between the shear and surface tension forces. In fact, the liquid shear stress on the wall is responsible for the film deposition while the surface tension force tries to keep the liquid from distributing. In terms of the shear stress underneath the liquid plug and its extension on the wall, there are three different zones as depicted in Fig. 6 including Developed, Meniscus transition, and Film zones. In the Developed zone, which is within the liquid plug, the flow is like a single-phase flow with a finite shear stress whose contribution in the total friction depends on the length of the liquid plug. An increase in the shear stress in the Meniscus Transition zone is observed, which is due to the meniscus curvature. As shown in Fig. 6 the curvature of the meniscus makes the flow deviate toward the wall and increases the axial velocity in this region. Moreover, the wavy shape of the interface, makes the shear profile fluctuate slightly. In addition, there are some recirculating flows within the film zone far from the meniscus nose in the deposited liquid film which leads to a locally negative profile of the shear stress. This kind of recirculating flow is specially observed in thicker liquid film which corresponds to higher capillary number. Recirculation of flow within the film zone was observed before [11], and could be a favourable phenomenon in terms of heat and mass transfer within the film region since it reduces the thermal resistance of the liquid film.

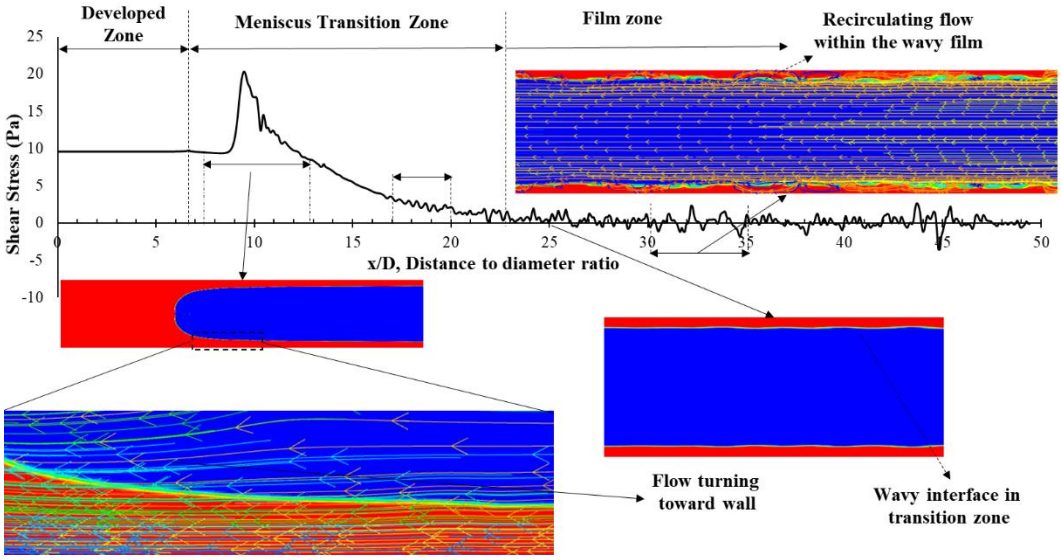

Fig 6: The shear stress profile and flow pattern at Ca=0.022

At low capillary numbers as shown in Fig. 7, the air momentum above the liquid film is not enough to pull the liquid film and that's why it's almost immobile with near zero shear stress underneath. However, at higher capillary numbers, the film thickness is thicker and due to the inertia, the liquid velocity as well as the shear stress profile approaches to zero more gradually. Besides, as presented in Fig. 7 the transition region from the meniscus to the film region is more gradual.

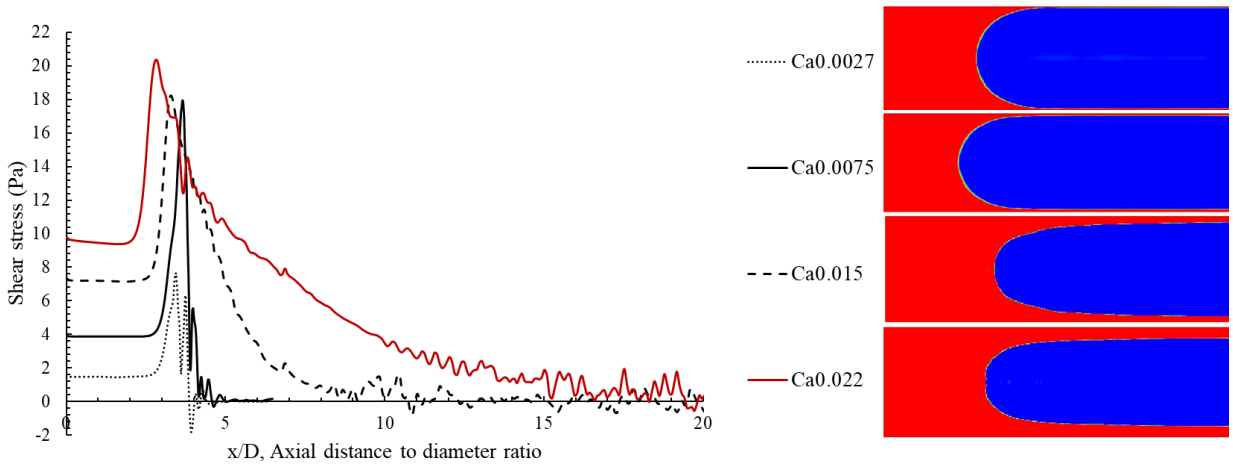

Fig 7: Shear stress profile at different capillary numbers

4. Conclusion

The CFD method with the approach of VoF was used to capture the deposited film behind a laminar receding meniscus in a capillary tube. Due to the requirement of a high grid resolution near the interface, the over set technique with a finite length moving domain of high grid resolution was used, to follow the meniscus to reduce the total number of computational cells and the computational time. The numerical results in terms of film thickness shows a very good match in comparison with the experimental data which means the CFD-VoF coupled with the overset grid generation yields acceptable results for wetting dynamics of such a flow. Moreover, the shear stress profile shows peak values near the meniscus and gradually drops down to zero in the film region. However, in the film region, some flow recirculation was observed which makes the shear profile fluctuating between small negative and positive values. The recirculating flow within the film region could have a favourable effect on the heat and mass transfer within that region. This is the first step toward complete and accurate modelling of an oscillating meniscus in a capillary tube, which includes mass and heat transfer as well.

References

[1] W. Jiansheng, W. Zhenchuan, and L. Meijun, "Thermal performance of pulsating heat pipes with different heating patterns," *Applied Thermal Engineering*, vol. 64, no. 1–2, 2014, doi: 10.1016/j.applthermaleng.2013.12.004.

[2] "Oscillating Heat Pipes."

[3] A. Nikkhah, A. Tessier-Poirier, N. Karami, O. Abouali, and L. G. Frechette, "Investigation of the Liquid Plug Friction Force in the Self-Oscillating Fluidic Heat Engine (SOFHE)," 2020. doi: 10.1109/powermems49317.2019.92321106939.

[4] J. G. Monroe, M. Bhandari, J. Fairley, O. J. Myers, N. Shamsaei, and S. M. Thompson, "Energy harvesting via thermo-piezoelectric transduction within a heated capillary," *Applied Physics Letters*, vol. 111, no. 4, 2017, doi: 10.1063/1.4996235.

[5] T. Monin, A. Tessier-Poirier, E. Léveillé, A. Juneau-Fecteau, T. Skotnicki, F. Formosa, F. Formosa, S. Monfray, L.G. Fréchette, "First experimental demonstration of a Self-Oscillating Fluidic Heat Engine (SOFHE) with piezoelectric power generation," in *Journal of Physics: Conference Series*, 2016, vol. 773, no. 1. doi: 10.1088/1742-6596/773/1/012039.

[6] J. G. Monroe, O. T. Ibrahim, S. M. Thompson, and N. Shamsaei, "Energy harvesting via fluidic agitation of a magnet within an oscillating heat pipe," *Applied Thermal Engineering*, vol. 129, 2018, doi: 10.1016/j.applthermaleng.2017.10.076.

[7] Q. Shen, C. Chang, P, Tao, Z. Ning, S. Rong, Y. Liu, C. Song, J. Wu, W. Shang, T. Deng, "Waste heat recovery in an oscillating heat pipe using interfacial electrical double layers," *Applied Physics Letters*, vol. 112, no. 24, 2018, doi: 10.1063/1.5033347.

[8] X. Zhang, V. Nikolayev, and V. S. Nikolayev, "Liquid film dynamics during meniscus oscillation," 2021. [Online]. Available: https://hal.archives-ouvertes.fr/hal-03388046

[9] Y. J. Youn, K. Muramatsu, Y. Han, and N. Shikazono, "The effect of bubble deceleration on the liquid film thickness in microtubes," *International Journal of Heat and Fluid Flow*, vol. 58, 2016, doi: 10.1016/j.ijheatfluidflow.2016.01.002.

[10] J. U. Brackbill, D. B. Kothe, and C. Zemach, "A continuum method for modeling surface tension," *Journal of Computational Physics*, vol. 100, no. 2, 1992, doi: 10.1016/0021-9991(92)90240-Y.

[11] E. Adaze, H. M. Badr, and A. Al-Sarkhi, "CFD modeling of two-phase annular flow toward the onset of liquid film reversal in a vertical pipe," *Journal of Petroleum Science and Engineering*, vol. 175, 2019, doi: 10.1016/j.petrol.2019.01.026.